Eur. Phys. J. AP **20**, 151–158 (2002)
DOI: 10.1051/epjap:2002086

THE EUROPEAN PHYSICAL JOURNAL
APPLIED PHYSICS

Study of the interaction between heavy ions and integrated circuits using a pulsed laser beam*

D. Lewis[a], P. Fouillat, V. Pouget, and H. Lapuyade

IXL, ENSEIRB-Université Bordeaux 1, 33405 Talence, France

Received: 20 November 2001 / Received in final form: 16 July 2002 / Accepted: 25 July 2002
Published online: 25 October 2002 –

Abstract. A new pulsed laser beam equipment dedicated to the characterization of integrated circuit is presented. Using ultra-short laser pulses is a convenient way to simulate experimentally the spatial environment of integrated circuits when interactions with heavy ions occur. This experimental set-up can be considered as a complementary tool for particle accelerators to evaluate the hardness assurance of integrated circuits for space applications. These particles generate temporally electrical disturbance called Single Event Effect (SEE). The theoretical approach of an equivalence between heavy ions and a laser pulses is discussed. The experimental set-up and some relevant operational methodologies are presented. Experimental results demonstrate that the induced electrical responses due to an heavy ion or a laser pulse are quite similar. Some sensitivity mappings of integrated circuits provided by this test bench illustrate the capabilities and the limitations of this laser-based technique. Contrary to the particle accelerators, it provides useful information concerning the spatial and temporal dependences of SEE mechanisms.

PACS. 85.40.Qx Microcircuit quality, noise, performance, and failure analysis

1 Introduction

Laser testing of Integrated Circuits (ICs) is a contactless and a non-destructive technique, which provides information on failure mechanisms and fault localization and allows successfully several mature ICs characterization methodologies.

Focusing a laser beam with a spot size less than 1 μm on to the device under test allows investigation with a spatial resolution suitable to the typical size of ICs.

Using ultra-short laser pulses with duration shorter than the electrical response time of the device provides relevant information in the time domain, for instance relaxation time and propagation time of the electrical response through the IC. These information allow the development of new methodologies for ICs characterization.

In space and nuclear applications, high-energy radiation may interact with integrated circuits leading to various kinds of failures and errors. For example, the passage of an unique ion through the device induces numerous transient effects grouped together under the name of single event effects (SEE). The characterization of SEE-hardened technologies usually implies to simulate the radiative context by using particles accelerators, which is expensive and not easily accessible. Moreover, this testing method doesn't allow some advanced information like spatial or temporal dependencies of SEE sensitivity.

In this context, using ultra-short laser pulses to deposit the same energy as an heavy ion provides a complementary tool that simulates the radiation effects in ICs.

In the first section the theoretical approach concerning the generation of photo-carriers with an ultra-short laser pulses is discussed and compared to the one obtained with heavy ions. In the second section the experimental equipment is presented. In the third section experimental results illustrate the usefulness of the laser methodology.

2 Theoretical approach

2.1 Single event effect in integrated circuit

An SEE is an electrical perturbation caused by the passage of a single ionizing high-energy heavy ion. When an energetic particle strikes an integrated circuit, the deposited energy generates within the context of Coulombian interaction in electron-hole pairs. The carriers collected at a sensitive node of the circuit induce a transient disturbance of electrical parameters which depends on the bias conditions and which is called Single Event Transient (SET). When the collected charge is sufficient, other effects occurs, such as the Single Event Upset (SEU) in digital circuits, the inversion of a binary information in digital circuits, and the Single Event Latchup (SEL), that consists in a short circuit between the power lines of the device.

* This paper has been first presented orally at the C2I colloquium in February 2001

[a] e-mail: lewis@ixl.u-bordeaux.fr

2.2 Simulating a SEE with a laser pulse

2.2.1 Introduction

A pulse of laser and a heavy ion both induce a transient generation rate of electron-hole pairs in a semiconductor. The heavy-ion and pulsed laser induced generation rates are intrinsically different due to the different nature of Coulombian and photoelectric interactions. The resulting carrier distribution induced by a laser pulse is also affected by the optical resolution due to the diffraction limitation.

However, despite the difference characteristics of these generation rates, experimental investigations and numerical simulations have shown that these two kinds of excitation produce similar transient effects in integrated circuits [1,2].

We have developed numerical simulations, which permit to compare the induced generation rate induced by an heavy ion and by a laser pulse.

2.2.2 Heavy ion tracks

For a heavy ion, the generation rate is defined by the initial energy and essentially by the linear transfer energy (LET) of the ion, this parameter represent the deposited energy per length unit. One commonly used model for describing the heavy ion induced generation rate in numerical device simulations is the Gaussian cylindrical model [3]:

$$g_{\mathrm{ion}}(r,z,t) = \frac{1}{\pi^{\frac{3}{2}} r_0^2 \tau_{\mathrm{rad}}} \frac{L_{\mathrm{i}}}{E_{\mathrm{p}}} \mathrm{e}^{\frac{r^2}{r_0^2}} \mathrm{e}^{-\frac{t^2}{\tau_{\mathrm{rad}}^2}}. \quad (1)$$

The L_{i} parameter represents the initial LET at the surface of the irradiated semiconductor. The r_0 parameter defines the radius of the cylindrical generation rate and is usually arbitrarily fixed to a typical value of 0.1 μm. The E_{p} parameter represents the average energy (3.6 eV in Si) to create a hole-electron pair.

The temporal aspect of the propagation can usually be neglected and the temporal variation of the generation rate is a global Gaussian profile. Its duration, τ_{rad}, includes the time of flight across the structure for the ion and the secondary electrons as well as the relaxation time of the generated carriers. It is of the order of 1 ps.

Figure 1 presents the charge track induced by a 275 MeV Fe ion, typical of the cosmic rays component of the space radiation environment. For this model the generation rate is assumed to be uniform along the propagation direction.

2.2.3 Laser pulse ion track

Considering a pulsed laser beam focused on the surface of a semiconductor the generation rate of electron-hole pairs

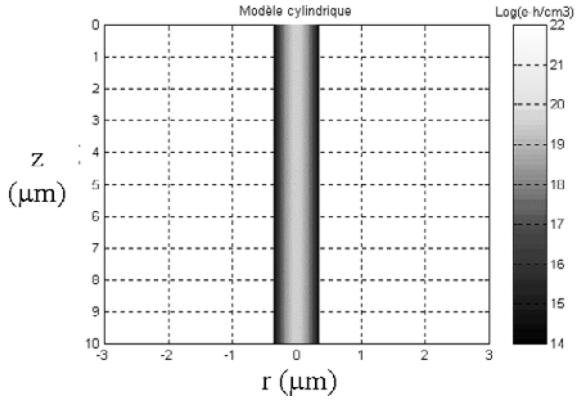

Fig. 1. Cylindrical model for heavy ion induced carrier densities defined by: $\int_{t=-\infty}^{t=+\infty} g_{\mathrm{ion}}(r,z,t)\mathrm{d}t$.

derived from the Beer-Lambert's law [4] is:

$$g_{\mathrm{las}}(r,z,t) = \frac{2\alpha T E_{\mathrm{L}}}{\pi^{\frac{3}{2}} \omega_0^2 E_\gamma \tau_{\mathrm{las}}} \frac{\omega_0^2}{\omega(z)^2} \mathrm{e}^{-\frac{2r^2}{\omega(z)^2}} \mathrm{e}^{-\alpha z} \mathrm{e}^{-\frac{t^2}{\tau_{\mathrm{las}}^2}} \quad (2)$$

$$\omega(z) = \omega_0 \sqrt{1 + \left(\frac{z}{z_{\mathrm{sc}}}\right)^2}. \quad (3)$$

The lateral profile is described by a Gaussian function in accordance with the fundamental transversal propagation mode of a laser beam. The ω_0 parameter is defined as the beam-waist located on the surface of the semiconductor. In accordance with Beer-Lambert's law, the intensity of the laser light decays exponentially with distance due to the absorption of the light. The parameter α is the optical absorption coefficient of the semiconductor. E_{L} is defined as the energy of the laser pulse, E_γ represents the energy of a photon and T is the energy transmission coefficient of the surface of the semiconductor. The parameter T may include interference effects in the oxide layer.

Because the circuit response is much longer than the propagation time of the laser pulse in the structure, the coupling between spatial and temporal variations is neglected and the temporal profile of the generation rate simply reproduces the temporal profile of the pulse. It is assumed to be Gaussian with a width of 1 ps in typical experimental condition [5].

Figure 2 presents the spatial distribution of hole-electron pairs (time-integrated generation rate) induced by a laser pulse for a wavelength of 0.8 μm and a transmitted energy of 8 pJ. The beam is assumed to be focused down to a spot size of 1 μm, near the theoretical diffraction limit imposed by the wavelength value. For the considered wavelength, most of the energy is absorbed before the beam spreading becomes significant.

2.2.4 Discussion

Figures 1 and 2 show the differences between laser and ion induced charge tracks. Contrary to the heavy ion case, the attenuation of the laser beam along the propagation

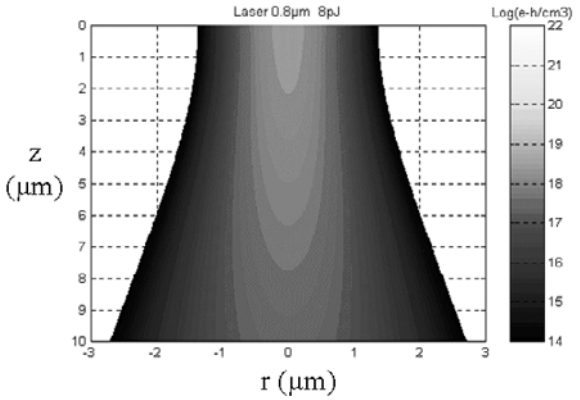

Fig. 2. Classical model for laser beam induced carrier densities defined by: $\int_{t=-\infty}^{t=+\infty} g_{\text{las}}(r,z,t)\mathrm{d}t$.

direction can not be neglected, the radial distribution is wider and the peak value is smaller. Nevertheless, when considering the problem at the scale of a whole circuit, a functional block, or even a single device, both ion and laser induced carrier distributions have very highly localized concentrations induced by transient interactions, and they are known for inducing similar single event effects. Numerical models have been brought into play in the goal to establish theoretical equivalence between the two generation rates [5]. By considering the experimental results presented in this paper, one can validate this theoretical approach with the comparison of electrical responses obtained for both cases.

2.2.5 Optical parameters choice

The most important optical parameter is the optical absorption, which is strongly governed by the laser wavelength. The literature presents several studies to estimate the optimum wavelength choice [1,6] for our kind of experiment. To approach the physical interaction between the device and an heavy ion, a convenient way is to select a laser wavelength able to provide a quite uniform longitudinal generation rate within the field of the active regions of the device under test. More over, a sufficient peak value for this generation rate to induce the single event effect (SEE) is required.

Due to the propagation mode of the laser in the lateral direction and due to the Beer-Lambert law along the vertical direction, the induced photo-carriers are chiefly located in a volume limited by its beamwaist (ω_0) and penetration depth ($1/\alpha$).

Table 1 presents different values of the laser penetration depth and the optical absorption *versus* wavelength laser [8,9]. By increasing the wavelength value up to 1.06 μm, one can obtain a quasi uniform generation rate but, for a given energy, the generation rate peak value is decreasing in the sensitive volume and should be not sufficient to induce a significant transient response.

In modern technologies, active devices within an integrated circuit are located in the vicinity of the silicon surface. Generally, the depth of the active structure is about

Table 1. Absorption coefficient and laser penetration depth for different wavelength values [8,9].

	$\lambda_0 = 0.8$ μm	$\lambda_0 = 1$ μm	$\lambda_0 = 1.06$ μm
Absorption coefficient (cm^{-1})	800	60	10
Penetration depth (μm)	12.5	167	1000

1 μm. In such a context, only photo-carriers generated within the very few micrometers under the surface are able to interact with the electronic function, since recombination phenomenon will dominate the behavior of the other induced carriers. Following down that road, the laser energy has to be deposited in this effective volume. If the aim is to approach the heavy ion induced distribution of hole-electron pairs, with an important penetration depth, we are leading to use red or infrared lasers, according to the data of Table 1.

A first limit comes from the fact that the use of greater wavelengths necessitates an increase of the laser energy to balance the decrease of the linear absorption coefficient. The drawback lies in the triggering of non linear phenomena, as the two photon absorption one. Then, the total number of generated carriers is less than in the linear case since it takes globally more than one photon to create an electron-hole pair.

Secondly, the laser beam is focused on the integrated circuit using a microscope objective. Considering the theoretical limit given by diffraction mechanisms and the objective microscope number of aperture NA, the minimum spot diameter of the circuit is given by:

$$d_0 \approx \frac{\lambda_0}{NA} \cdot \tag{4}$$

According to these two limits, new infrared lasers are well suited, and such a choice is made easier due to available commercial equipments. By reducing the wavelength close to 0.8 μm one can reduce the spot size down to 1 μm. To optimize the both criteria the value of 0.8 μm is selected. This choice is validated by the following experimental studies presented in this paper.

The second parameter is the pulse duration. One can assume that the fastest electrical time response of the SEE mechanism is restricted by the dielectric relaxation time, which is close to 1 picosecond in the silicon. Pulse duration close to 1 ps is selected. More over, this value is in accordance with the time constants commonly used with heavy ions.

2.2.6 Limitations

Contrary to a heavy ion, a laser beam focused on the front side of the device is stopped by the metalization layers. In the case of very large scale integrating (VLSI) circuits with multi-level metalization, it is often difficult or even

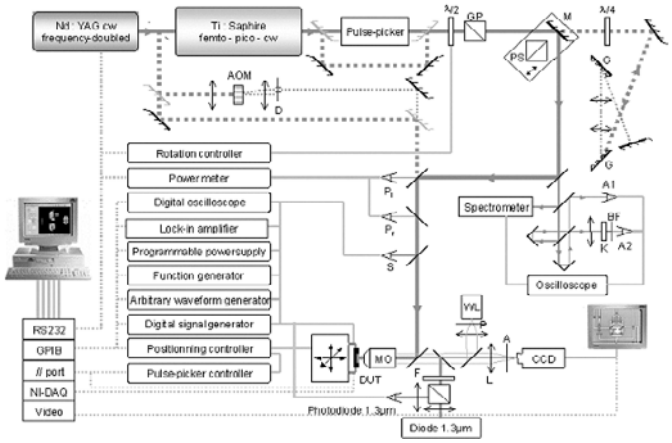

Fig. 3. Pulsed laser set-up for SEE testing.

impossible to perform the traditional front side laser testing since. To overcome this major limitation of the laser technique, backside technique is required, *i.e.* the laser is focused to the backside of the device, propagates through the substrate and reaches the sensitive regions with a sufficient energy to induce an SEE. Backside techniques are currently under investigation with some promising results [10,11].

3 Experimental set-up

Figure 3 presents a scheme of the pulsed laser set-up, used for SEE sensitivity evaluation. The basic experimental set-up is based on a Ti:Sapphire pulsed laser delivering ultra-short pulses. The pulse repetition rate varies from single-shot to 80 MHz using a pulse-picker. At the output of the pulse picker two pulse durations are available: 500 fs and 1 ps. And additional pulse stretcher compressor allows to vary pulse duration from 100 fs to 20 ps. The wavelength is tunable from 750 nm to 1080 nm.

The beam is focused down to a spot size of 1 μm on the surface of the device under test with an $\times 100$ or a $\times 50$ microscope objective ($NA = 0.8$). The minimum spot size can be roughly estimated to 1 μm from the numerical aperture of the objective for a given wavelength of 0.8 μm. But a precise measurement should take into account the non-perfectly Gaussian propagation of the beam, by determining both the divergence of the beam and its radius (the beam-waist) in the focal plane. This spatial calibration of the beam is achieved by a knife-edge technique [12], which gives a precision of 0.1 μm on the measured beam-waist. The experimental value obtained with this technique is close to 1 μm.

The device under test (DUT) is mounted on a three-dimensional translation stage, allowing a 0.1 μm moving resolution. The spatial distribution of the laser beam energetic density is well known: the lateral repartition is a Gaussian. Thus, after a deconvolution, the spatial resolution of the technique may be brought back to the minimum step of the moving table.

The selected pulse energy is automatically adjusted with a motorized half plate ($\lambda/2$) and a polarized prism (P).

For applications such as SEE hardness assurance, where energy threshold measurements are involved, it is necessary to accurately estimate the fraction of the incident pulse energy that has been really absorbed by the device, which implies a rigorous measurement of the reflected energy. This is obtained in line with two detectors providing a pulse to pulse monitoring of the incident to reflected energy ratio. The relative measured values have to be converted to absolute ones by advanced calibration procedures, which must include, for example, absorption in the objective and diffuse as well as normal reflection on the device.

A collimated white light beam is merged into the laser beam path to illuminate the circuit surface. The reflected light is collected by a CCD camera and can then be used for visualization of the laser spot on the device. Precautions must be taken with the visualization system so that the geometric image plane really corresponds to the plane in which the Gaussian laser beam is focused. For backside analysis, an additional visualization system including a continuous wave 1.3 μm laser with 6 mW power based on infrared (IR) backside scanning reflectometry measurement has been built. The resulting reflectometry map permits to obtain an image of the device layout.

A particular effort was made on the automation of the whole system, which can be synchronized up to a frequency of 1 kHz (including scan motions). This way, a sensitivity map of 100 k points for 10 different pulse energies is obtained in less than 30 minutes for simply controlled circuits.

4 Experimental results

4.1 SET analysis

4.1.1 Device under test

The acronym SET for Single Event Transient represents the temporary variation of any electrical parameter induced by the passage of an unique heavy ion through the electronic device. This phenomenon is currently an essential issue, specially for linear integrated circuits involved in space applications [13]. As an example for this presentation, the device under test is a commercial quadruple amplifier operational LM124 from National Semiconductor. This device is known to be widely used in space programs. For our purpose, only one of the four amplifiers is used and connected as a voltage amplifier.

4.1.2 Experimental validation of the equivalent effects induced by a laser pulse and an heavy ion

In this experiment, the output voltage of the amplifier is under study. Figure 4 presents comparison of the transient response obtained with a particle accelerator (boron

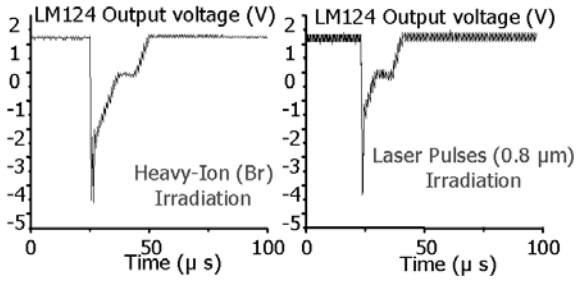

Fig. 4. LM124 transient responses for an ion strike and a laser pulse strike [13].

ion) at the Nuclear Physics Institute in Orsay and with our pulsed laser equipment. Both signals present the same temporal shape. For this, the laser beam has been focused with a $\times 50$ microscope objective and the spot diameter was 2 μm at the surface of the device. Although the generation rates are different for both the laser pulse and the heavy ion, we can observe great similarities between the electrical responses. These results demonstrate the ability to simulate with pulsed laser heavy ion effect for this kind of circuits.

4.1.3 Analog mappings

In the case of SET studies, the following procedure is performed to obtain automatically analog maps of the transient response. The scan window and the step size are preliminary defined in a two dimensional grid. For each point of the grid, the motorized axes are stopped and n pulses are fired. A 1 GHz bandwidth digital oscilloscope acquires the transient signals and computes the average one from the n sweeps. A predetermined set of electrical parameters of the induced signal is then stored, selected among the following ones: maximum, RMS, peak to peak, rise time, Fast Fourier Transform, etc. For each parameter, a two dimensional representation is built by associating the measured values to a color scale. In this mode of operation, the influence of hazardous variations of pulse energy is attenuated, but the duration of the scan process is n times longer. Calculation and acquisition stages only limit the speed scan.

Figures 6 and 7 present the results for front side SET analysis obtained on a LM124 (see Fig. 5), operating as an inverting amplifier. The duration of one laser pulse is about 1 ps, the wavelength is 0.8 μm, and the energy per pulse is 10 pJ. The parameters under study are respectively the maximum, and the peak to peak value. These mappings are then analyzed to identify the most sensitive part of the electronic function. The major limitation due to the metallic tracks occulting the laser beam is clearly observed. Nevertheless, for this kind of integrated circuits, the metal track density is quite low and the laser beam method provides essential and complementary information to localize precisely the SET sensitive zones.

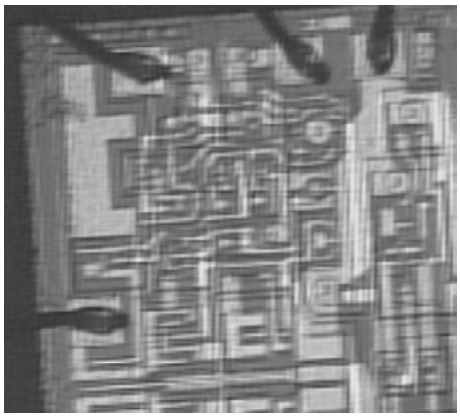

Fig. 5. Microphotography of the LM124 scanned area.

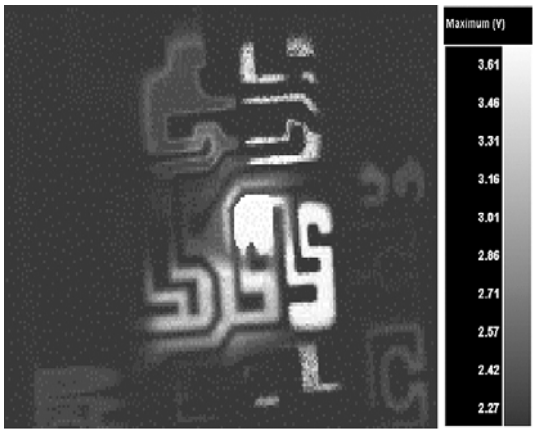

Fig. 6. Map of the maximum of the transient response.

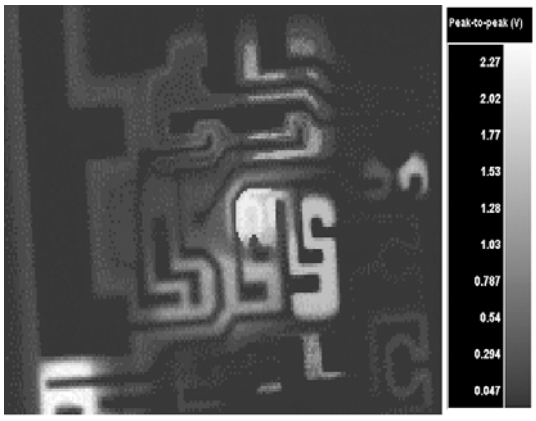

Fig. 7. Map of the peak to peak value of the transient response.

4.2 SEU analysis

4.2.1 Device under test

Figure 8 presents a test vehicle designed to study the behavior of a basic memory cell design for space application. Our main goal was to understand the mechanisms responsible for the change of the binary data stocked in the cell when an ion strike occurs. The chip was designed with 0.8 μm AMS BiCMOS technology (NMOS in the bulk).

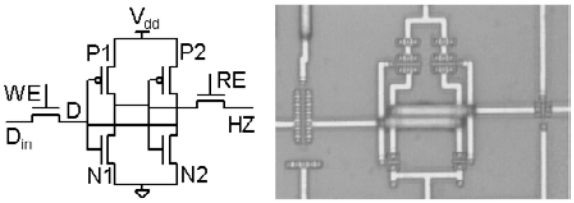

Fig. 8. Electrical schematic and microphotography of the tested basic SRAM cell.

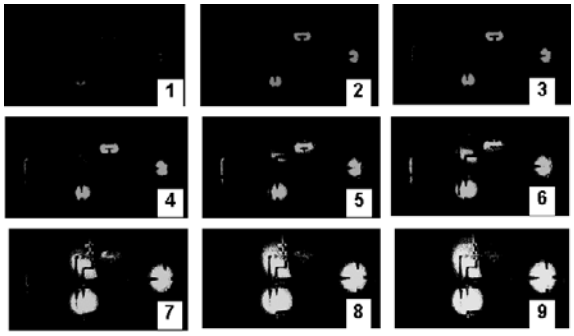

Fig. 9. SEU sensitivity maps for increasing energies.

To minimize the influence of the spot size comparatively to the transistor size and to properly evaluate the influence of the different internal regions, we have deliberately spaced the distance between each elementary component of the electronic function. This test vehicle is well suited for a fundamental study because of the low density of metallic tracks.

4.2.2 SEU mappings

In the case of single event effect (SEU) studies the following procedure is brought into play. The scan window and the step size are preliminary defined in a two dimensional grid. The cell is initialized in a given state and the scan velocity is selected. The laser continuously inspects a row of the grid and the laser pulses are directly synchronized by the positioning control system which delivers electrical pulses corresponding to each selected node of the grid. For each point, an unique laser pulse is fired. The state of the cell is then read and reinitialized if corrupted. For each strike location that induces an upset (SEU), the corresponding point is colored on a 2D map.

Figure 9 presents different SEU mappings for a given logical state of the same area for different incident energies. The step size of the scan is 0.2 μm. The SEU sensitive area increases with the incident energy.

4.2.3 SEU cross section

By integrating the sensitive area of each map, we obtain the curve depicted in Figure 10. The nine points of this curve correspond to the nine maps of Figure 9. In the goal to perform this integration stage the laser-scanned area S is divided in $M \times N$ elementary pixels. The M and N values are obtained by dividing the dimensions of the scan window by the step size of the scan. By counting the number N_E of induced events (*e.g.* upsets) for a given pulse energy, a simple formula is obtained:

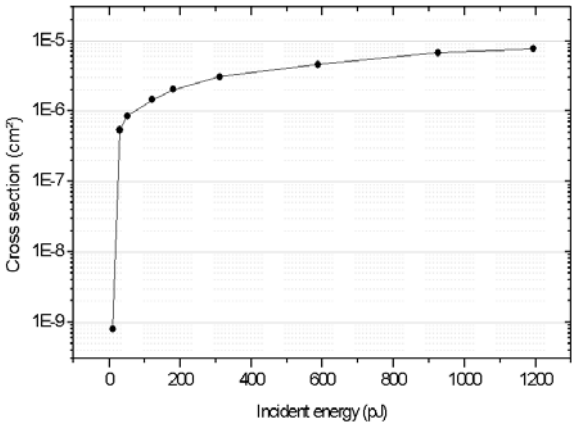

Fig. 10. Experimental laser cross section for the extracted from the maps of Figure 10.

$$\sigma_{\mathrm{L}}(E_{\mathrm{L}}) = \frac{S}{M \times N} N_E(E_{\mathrm{L}}) \tag{5}$$

where σ_{L} is defined as a SEU laser cross section and E_{L} the incident energy.

The laser cross section curve has the same behavior as the classical heavy ion cross section curves. By this way it is then possible to extend the cross section notion used in particles accelerator testing to the pulsed laser testing [14]. In the case of heavy ion interaction, the curve presents the cross section behavior *versus* the heavy ion linear transfer energy (LET). The main limitation of the laser method is to correlate the laser energy E_{L} to the heavy ion LET in the goal to define an equivalent laser LET which is technology independent and which is not affected by the metallic tracks.

Nevertheless, the laser method provides rapidly preliminary results concerning the SEU sensitivity of integrated circuit. For example one can study the influence of the logical state on the SEU sensitivity.

Figure 11 summarizes the results for four different electrical conditions. In each picture, the maps for the different energies are superimposed. It allows a global vision of the SEU sensitivity.

For instance, according to the maps presented in Figure 11, we can identify some particular sensitive areas such as the drain/bulk reverse-biased junction of the blocked MOS transistor, as well as the contribution of the WE and the RE transistors to the global sensitivity of the device. Recent studies published in reference [15] have explained the basic mechanisms attached to these experimental results.

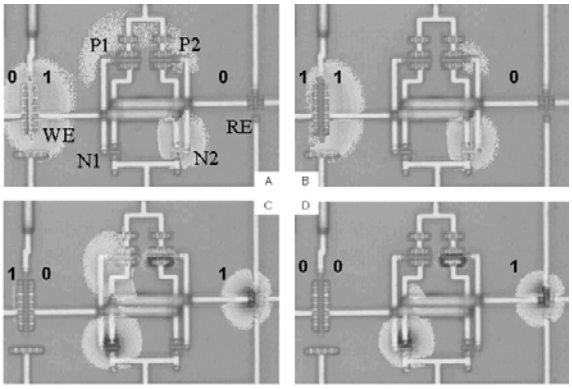

Fig. 11. Sensitivity maps of the single SRAM cell for different logical states.

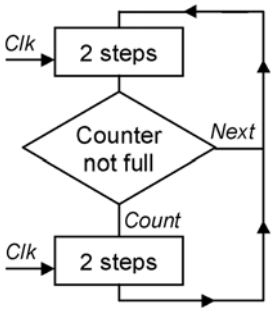

Fig. 12. Principles of the tested sequencer. *Count* and *Next* are observed with respect to *Clk* to detect an error.

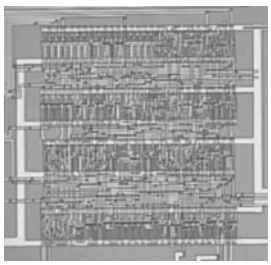

Fig. 13. Counter-sequencer under test.

4.3 Dynamic SEU analysis

The pulsed laser equipment is also a powerful tool for error injection into a circuit or a system with an accurate spatial and temporal positioning. To illustrate this feature, we have tested a counter-sequencer, part of a neuronal application circuit.

Figure 12 presents the principle of the tested function. The sequencer first operates two steps on the falling edge of a clock. A 4 bit counter is then incremented (*Count* signal) if not full yet and two more steps are performed. If the counter is already full, the sequence is reinitialized (*Next* signal). The chronogram in normal operations is thus the following: 4 *Clk* periods between each *Count*, and 16 *Count* between each *Next*.

Figure 13 presents a microphotography of the device under test.

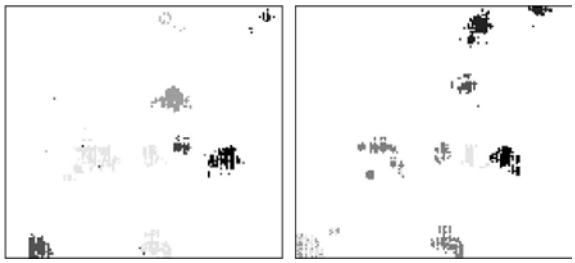

Fig. 14. Dynamic error maps for two different trigger times.

Figure 14 presents two dynamic SEU maps, each map corresponds to one different trigger time in the sequence, when the laser pulse strikes the device. Each gray level intensity corresponds to one particular type of error (count error, reset...). In both maps the same sensitivity areas are observed. It is important to notice that for one particular area the error signature could be different. Due to the complexity of the tested device, it is difficult to provide a simple interpretation concerning these experimental results without a reverse engineering investigation which must be followed by a static or a dynamic modeling step. These maps reveal that this testing method provides essential information concerning the temporal dependence of the radiation sensitivity and allows extracting experimentally time window sensitivity. This methodology has been successfully brought into play to study the temporal dependence of the SEU sensitivity on a commercial DRAM memory [16] and to study the error sensitivity of a CAN (experiments in progress).

5 Conclusion

We have experimentally demonstrated, that the laser technique is mature and is a good candidate to reproduce heavy ion environment in integrated circuits. Our experimental set-up which is entirely automated provides integrated circuit sensitivity maps with a spatial resolution well suited to currently used technologies for integrated circuits. It permits to obtain spatial information concerning the location of the sensitivity areas attached to a particular phenomena such as SET or SEU. The ability to synchronize precisely a laser pulse with the clock of the device under test allows also a dynamic investigation of the device behavior. Such an equipment offers a wide panel of test techniques on ICs for the quality and reliability characterization. Further study on real cases for defects and faults localization will be brought into play to validate the global testing methodology. In a very near future, the wavelength tunability will allow a wide panel of backside techniques to counteract the shielding effects due to front side metal tracks.

References

1. J.S. Melinger, S. Buchner, D. McMorrow, W.J. Stapor, T.R. Weatherford, A.B. Campbell, IEEE Trans. Nucl. Sci. **41**, 2574 (1994)

2. S.C. Moss, S.D. LaLumondiere, J.R. Scarpulla, K.P. MacWilliams, W.R. Crain, R. Koga, IEEE Trans. Nucl. Sci. **42**, 1948 (1995)
3. R.L. Woodruff, P.J. Rudeck, IEEE Trans. Nucl. Sci. **40**, 1795 (1993)
4. A.E. Sigman, University Science Books, Mill Valley, California (1986)
5. V. Pouget, P. Fouillat, D. Lewis, H. Lapuyade, S. Buchner, Microelectron. Reliab. **41**, 1513 (2001)
6. J.S. Melinger, D. McMorrow, A.B. Campbell, S. Buchner, L.H. Tran, A.R. Knudson, W.R. Curtice, J. Appl. Phys. **84**, 690 (1998)
7. K.W. Golke, IEEE Trans. Nucl. Sci. **40**, 1910 (1993)
8. M. Saritas, H.D. McKell, J. Appl. Phys. **61**, 4923 (1987)
9. A.H. Johnston, IEEE Trans. Nucl. Sci. **40**, 1694 (1993)
10. D. Lewis, V. Pouget, F. Beaudoin, P. Perdu, H. Lapuyade, P. Fouillat, A. Touboul, IEEE Trans. Nucl. Sci. **48**, 2193 (2001)
11. R. Desplats, F. Beaudoin, P. Perdu, P. Poirier, D. Tremouilles, M. Bafleur, D. Lewis, Microelectron. Reliab. **41**, 1539 (2001)
12. Y. Suzaki, A. Tachibana, Appl. Opt. **14**, 2809 (1975)
13. P. Adell, R.D. Schrimpf, H.J. Barnaby, R. Marec, C. Chatry, P. Calvel, C. Barillot, O. Moi, IEEE Trans. Nucl. Sci. **47**, 261 (2000)
14. V. Pouget, P. Fouillat, D. Lewis, H. Lapuyade, F. Darracq, A. Touboul, Microelectron. Reliab. **40**, 1371 (2000)
15. F. Darracq, T. Beauchêne, H. Lapuyade, D. Lewis, V. Pouget, P. Fouillat, *Proceedings of the RADECS conference (2001)*
16. S. Duzellier, D. Falguère, L. Guibert, V. Pouget, P. Fouillat, R. Ecoffet, IEEE Trans. Nucl. Sci. **47**, 2392 (2000)